



Statistical and Temporal Characteristics of Sawtooth Events

Connor C. DiMarco^{1,2}, Tuija I. Pulkkinen¹, and Michael G. Henderson²

¹University of Michigan, Ann Arbor, MI, USA

²Los Alamos National Laboratory, Los Alamos, NM, USA

Correspondence: Connor C. DiMarco (cdimarco@umich.edu)

Abstract. Magnetospheric sawtooth events are characterized by periodic particle injections and magnetic dipolarizations spread quasi-simultaneously across a wide range of magnetic local times. We present a comprehensive statistical study of magnetospheric sawtooth events (STEs) during solar cycle 24 (2008–2016), extending previous catalogs and enabling solar cycle comparisons. Our results confirm that STEs predominantly occur during the declining phase of the solar cycle and are strongly associated with geomagnetic storms. Superposed epoch analysis reveals near-simultaneous particle injections across all magnetic local time sectors but magnetic field dipolarization confined to the midnight region, supporting a scenario in which nightside tail reconnection and enhanced convection are the primary drivers. The localization of magnetic dipolarizations during STEs challenges global instability interpretations and suggest that STEs represent a stormtime substorm mode triggered under specific magnetotail conditions.

10 1 Introduction

Magnetospheric Sawtooth Events (STEs) have been described as periodic particle injections accompanied by magnetic dipolarizations, primarily observed from geostationary orbit (Henderson et al., 2006). While a strict definition of a sawtooth event does not exist, they are commonly identified by their qualitative features. Figure 1 shows a sample event, indicating quasi-simultaneous energetic particle injections around the globe. While several authors have addressed the characteristics and drivers of sawtooth oscillations (Henderson et al., 2006; Pulkkinen et al., 2007; Cai and Clauer, 2009; Fung et al., 2016), there are still major disagreements in both the definition of a sawtooth event and the physical processes that drive these phenomena.

Several different theories have been employed to describe STEs. Lee (2004) suggests that sawtooth oscillations are driven by solar wind and interplanetary magnetic field (IMF) fluctuations. They demonstrated that periodic behavior at geosynchronous orbit can be associated with periodic solar wind pressure pulses driving either periodic compressions or substorms in the magnetosphere. However, we note that there are sawtooth events that are not associated with periodic solar wind driving.

Furthermore, several scenarios have been employed for producing periodic global (from nightside to dayside) stretching and dipolarization of the dipole field. First, global stretching has been suggested to arise from increased pressure from the lobe magnetic field: As the cusps move sunward under polar-cap potential saturation, magnetic pressure from the northern and southern lobes on the dayside closed magnetosphere increases (Borovsky et al., 2009). Secondly, the dayside stretching has been associated with an increased plasma pressure and current in the dayside magnetosphere, created by strong convection from the nightside plasma sheet (Pulkkinen et al., 2006). Third, the dayside stretching has been associated with strong Region-1 (R1)



30

35

40



current under polar cap saturation conditions, weakening the dipole magnetic field in the dayside equatorial magnetosphere (Borovsky et al., 2009). Figure 1 shows a simple illustration of a possible magnetic field reconfiguration cycle. Here we perform a comprehensive assessment of the magnetic field evolution at geostationary distance during sawtooth events.

Lastly, it has been argued that the sawtooth injections are driven by the same mechanisms as substorms, and that periodic substorms and sawtooth events represent a continuum from weaker to stronger driving (Pulkkinen et al., 2007; Henderson, 2016). Although in some events dispersionless injections have been observed to reach all the way into the dayside geostationary orbit (Borovsky et al., 2004), it has been shown that in some cases these injections are in fact not dispersionless (Henderson et al., 2006), but only appear to be so due to the high drift speed during strong convection. Examination of the full energy spectrum including the lower energy plasma shows that these injections indeed are not completely dispersionless, but originate from the magnetotail where the dispersion signatures are smallest. This would suggest that sawtooth events might be a class of substorms with strong enough convection to exhibit global quasi-dispersionless energetic particle injections.

Prior statistical STE studies (Fung et al., 2016) all focus on time period prior to 2007. Here we return to the physics of sawtooth events by creating a comprehensive list of sawtooth events covering a full solar cycle (2008-2018), while comparing and complementing these observations with the prior studies focusing on the previous solar cycle. For the first time, we also analyze the magnetic field stretching and dipolarization in a statistical sense.

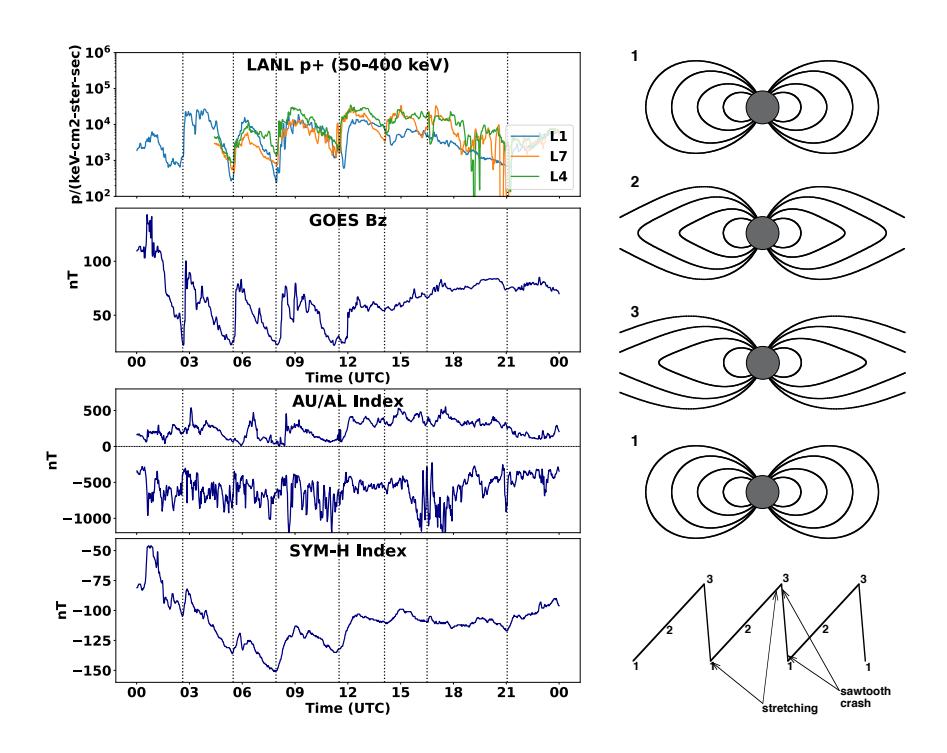


Figure 1. (left) Geosynchronous orbit ion fluxes and Bz, the AU and AL indices, and the SYM-H index during the April 18th 2002 sawtooth event. (right) Possible magnetic field change scenario associated with sawtooth events.





2 Data

45

Identification of sawtooth injections was done using the Los Alamos National Laboratory (LANL) GEOGRID data. The low-energy particle detector is designed to measure key plasma parameters such as density, temperature, and bulk velocity of ions and electrons at geosynchronous orbit (Bame et al., 1993). The instrument covers the low-energy plasma populations in the range of a few eV to several keV, providing insights into the dynamics of the background plasma environment during magnetospheric disturbances, and into dispersion patterns of the particle injections. The high-energy particle instrument measures the flux of energetic ions and electrons in the range of tens of keV to several MeV (Belian et al., 1992). The instrument is particularly suited for detecting energetic particle injections and enhancements during geomagnetic storms, substorms, and sawtooth events. We use the high-energy proton observations to identify sawtooth events, searching for periodic particle injections. The "sawtooth" signature is characterized by periodic sharp flux increases followed by slow decreases, observed simultaneously by the multiple spacecraft placed across a broad range of local times. Our study covers a 10-year period from 2008 to 2018, during which there are between 3 and 6 satellites available at varying longitudes of the geostationary orbit.

The vertical lines in Figure 1 show the start of the sudden increases of the fluxes, which we identify as the onset of the sawtooth injection.

The magnetic field dipolarizations during the sawtooth events can be observed in the magnetometer observations from the two geostationary orbit spacecraft located above the eastern and western US (Singer et al., 1996). Furthermore, for added longitudinal coverage, we use the field inclination deduced from the energetic particle distribution functions (Thomsen et al., 1996; Chen et al., 2016).

60 3 Methodology

We compiled a list of sawtooth injections by visual inspection of the LANL proton flux data from 100 to 500 keV. The energetic particle data was then combined with the SYM-H index from the OMNI database (Papitashvili et al., 2014) and magnetic field from the GOES spacecraft (Singer et al., 1996). For each event, we identified individual tooth onset times, with the tooth onset defined as the earliest time of the injection across the available spacecraft. It is important to note that this list was created using a qualitative process (visual identification), and may not include all of the sawtooth events that may have occurred during this time interval. The list of sawtooth events containing 81 events is provided in the Supplement (supplement.pdf).

We compare our results with a previous list of sawtooth events published by Cai and Clauer (2009), here referred to as CC09, that covers much of Solar Cycle 23 with a total of 111 sawtooth intervals containing 438 separate teeth. This study utilized a similar method of event identification; together the two lists cover almost two full solar cycles. Figure 2 shows the occurrence of sawtooth events in relation to the solar cycle, spanning 18 years of observations. The number of sawtooth events per year are shown with data from CC09 in blue and this study in red. Overlaid in gray is the yearly sunspot number, which provides a proxy for solar activity and solar cycle phase.

Sawtooth events show a strong positive correlation with the solar cycle, reinforcing the idea that the vast majority (95%) occur during geomagnetic storms (Cai et al., 2011; Cai and Clauer, 2009). Interestingly, the occurrence of sawtooth events





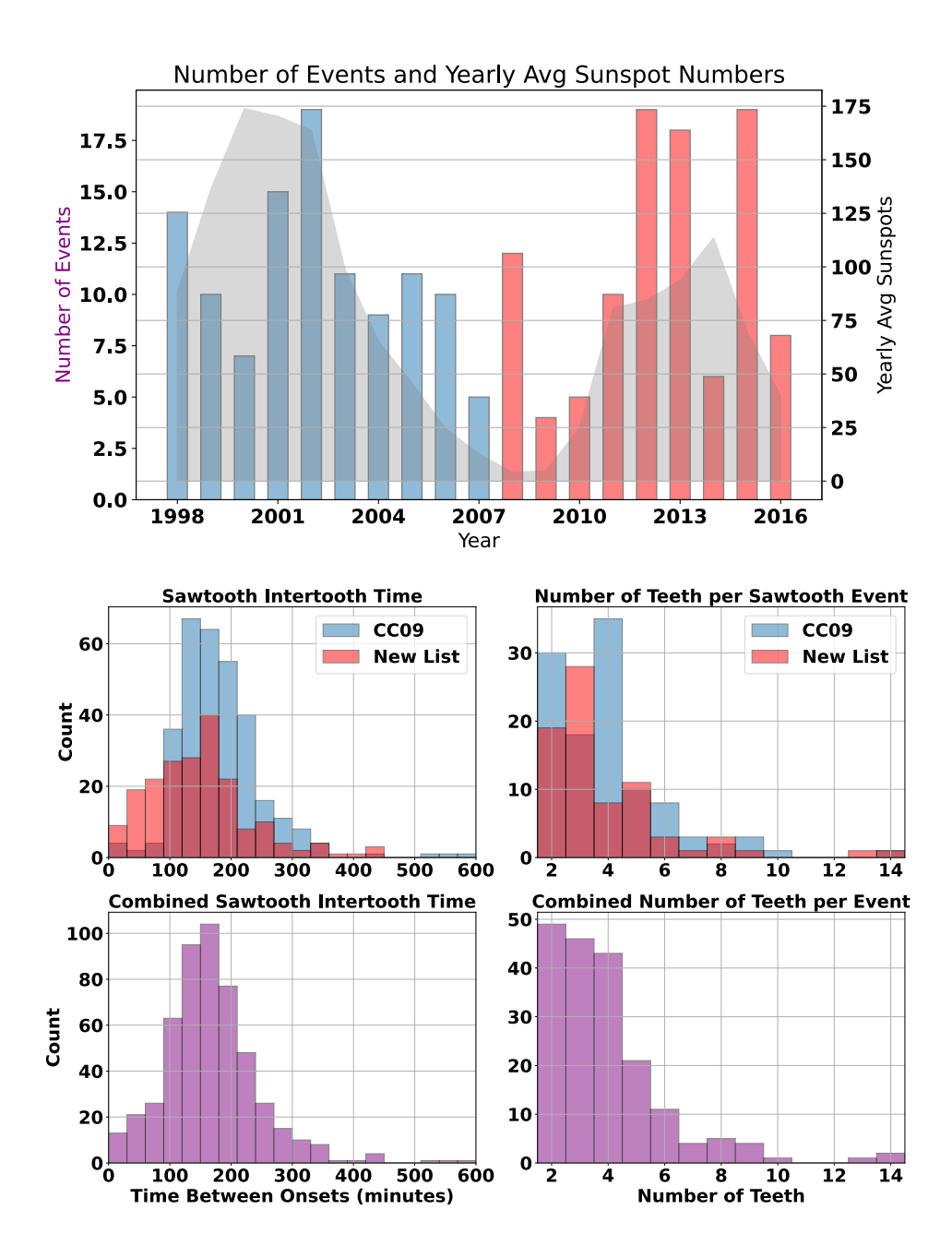


Figure 2. (top) Annual distribution of sawtooth event occurrence with the annual sunspot number on the background. (middle left) Average duration between two sawtooth injection onsets (intertooth interval) for this study (red) and CC09 (blue). (middle right) Average number of teeth per event for this study (red) and CC09 (blue). (bottom left) Combined average duration between sawtooth injections. (bottom right) Combined average number of teeth per event.





does not peak precisely at solar maximum but rather during the declining phase of the solar cycle – resembling the occurrence frequency of interplanetary coronal mass ejections (ICMEs) and magnetic clouds (Kilpua et al., 2011). For solar cycle 24, the vast majority of the events occur during geomagnetic storms.

The bottom panels of Figure 2 present a comparative analysis of sawtooth event characteristics across the CC09 time period and this study. The top-left panel shows the distribution of inter-tooth intervals, showing the time between two successive onsets, while the top-right panel shows the number of teeth per sawtooth event. Both distributions are presented for two datasets: the CC09 (blue) covering the period 1998–2008, and this study (red) covering the period 2008–2016. The two plots below show the combined distributions of intertooth times and number of teeth per sawtooth event.

The inter-tooth interval distributions reveal that during both periods, most events occur within 400 minutes (\sim 7 hours) the highest concentration of intervals below 200 minutes. However, our dataset exhibits a slightly broader distribution, with a higher frequency of longer intervals, suggesting a higher variability in event spacing and a potential bias in event selection. The distribution of teeth per sawtooth event shows that the majority of events contain 2-6 teeth, with a peak around 2–4 teeth. While both datasets exhibit similar overall trends, CC09 has a more pronounced peak at 4 teeth, whereas our events have a slightly wider spread, indicating more frequent occurrences of both low- and high-teeth events, or another potential selection effect. The intertooth interval peak at 160 min is consistent with the observed recurrence period of substorms of 2–4 hours (Borovsky and Yakymenko, 2017) and very close to the value obtained by Freeman and Morley (2004) for substorm recurrence of 2.7 hours.

4 Results

100

105

Figure 3 shows a superposed epoch analysis (SEA) of sawtooth event signatures at geostationary orbit in four magnetic local time (MLT) quadrants (09-15 MLT, 15-21 MLT, 21-03 MLT, and 03-09 MLT). The SEA algorithm calculates the mean behavior of a given quantity around an epoch time (here the sawtooth injection onset time). The SEA was applied to the proton and electron fluxes using linear averaging of the actual flux values. Similarly, the SEA was applied to the magnetic field inclination angle derived from the GOES magnetometers and LANL distribution functions. Because of the different instrumentation to calculate the field inclination, we show the LANL and GOES magnetic field results separately.

The superposed epoch analysis shows prompt increase of energetic proton and electron fluxes, with the nightside showing the first response, but the other three local time sectors showing rather similar enhancements after short delay times. Furthermore, the average magnitude of the flux increase is about the same in each quadrant, indicating that roughly the same population reaches the geostationary orbit at all local times.

The magnetic field inclination is compared with the quiet time value taken to be the T89 model using Kp = 2 (Tsyganenko, 1989). Note that the data from geostationary satellites include a diurnal sinusoidal variability as even during quiet times, the magnetic field is more stretched (smaller inclination angle) in the nightside and more compressed (higher inclination angle) in the dayside. Thus, one would expect the dawn and dusk sectors to show decreasing and increasing tilt angles, respectively, as



110

135



the spacecraft move eastward in their orbits, while the noon and midnight would show a maximum and minimum of the field, respectively. The T89 model results clearly demonstrate this diurnal variation.

In the midnight sector, the field is stretched, and stretches further during the hour prior to the onset. Following the injection, the field dipolarizes but does not reach the model field value, indicating that the tail and magnetospheric current systems have not completely reconfigured (Baker et al., 1996). The dawn and dusk fields, likewise, show a strongly stretched field, but only a minor field inclination change at the time of the injection. The dayside field is strongly compressed (more dipolar than model) prior to the injection, while the field is stretched following the arrival of the energetic particle population.

5 Discussion

In this study, we have identified sawtooth events using LANL energetic particle measurements from the period 2008 – 2016. Comparing with prior Cai and Clauer (2009) indicates that the characterizing properties of sawtooth oscillations, such as their recurrence intervals and the number of teeth per event, remain largely constant across the two solar cycles. This suggests that despite variations in solar wind conditions and geomagnetic activity, the underlying mechanisms governing sawtooth formation are robust.

Several open questions remain regarding the classification of sawtooth events and development of a more objective definition of this phenomenon. Geomagnetic activity is often described by empirically defined modes including storms, sawtooth events, substorms, steady convection events and pseudobreakups in decreasing order of intensity. While the "typical best cases" in each category have distinct features, there are overlaps and borderline cases that make accurate distinction challenging (Pulkkinen et al., 2010). However, even despite this overlap, the magnetospheric processes during each of these modes are sufficiently different that they need to be separately addressed in order to fully understand the complexity of the solar wind–magnetosphere–ionosphere coupling.

Bracketed by individual substorms and magnetic storms, there still is no well-defined threshold for the level of solar wind driving or required magnetospheric or ionospheric conditions necessary to trigger or suppress sawtooth oscillations. It is also noteworthy to mention that the global MHD simulations have not been able to reproduce the sawtooth event signatures to good level of accuracy. Previous modeling studies suggest that periodic behavior can be recreated either with strong O^+ flux (Brambles et al., 2011), or with kinetic reconnection in the magnetotail (Wang et al., 2022).

The solar cycle dependence of sawtooth events shows that they predominantly occur during the declining phase of the solar cycle, with little increase in occurrence near solar maximum. This suggests the existence of a threshold beyond which stronger solar wind driving may suppress the periodic sawtooth oscillations, possibly transitioning the magnetosphere into a different, more disturbed and potentially more directly driven state. This result is consistent with previous work on magnetospheric modes (Pulkkinen et al., 2007; Delzanno and Borovsky, 2022), which suggests that different levels of external driving can activate distinct large-scale responses in the system.

Using the LANL and GOES geostationary satellite datasets, we examined particle injections and magnetic field dipolarizations in different magnetic local time sectors (midnight, dawn, noon, dusk). Our analysis reveals that sawtooth events produce





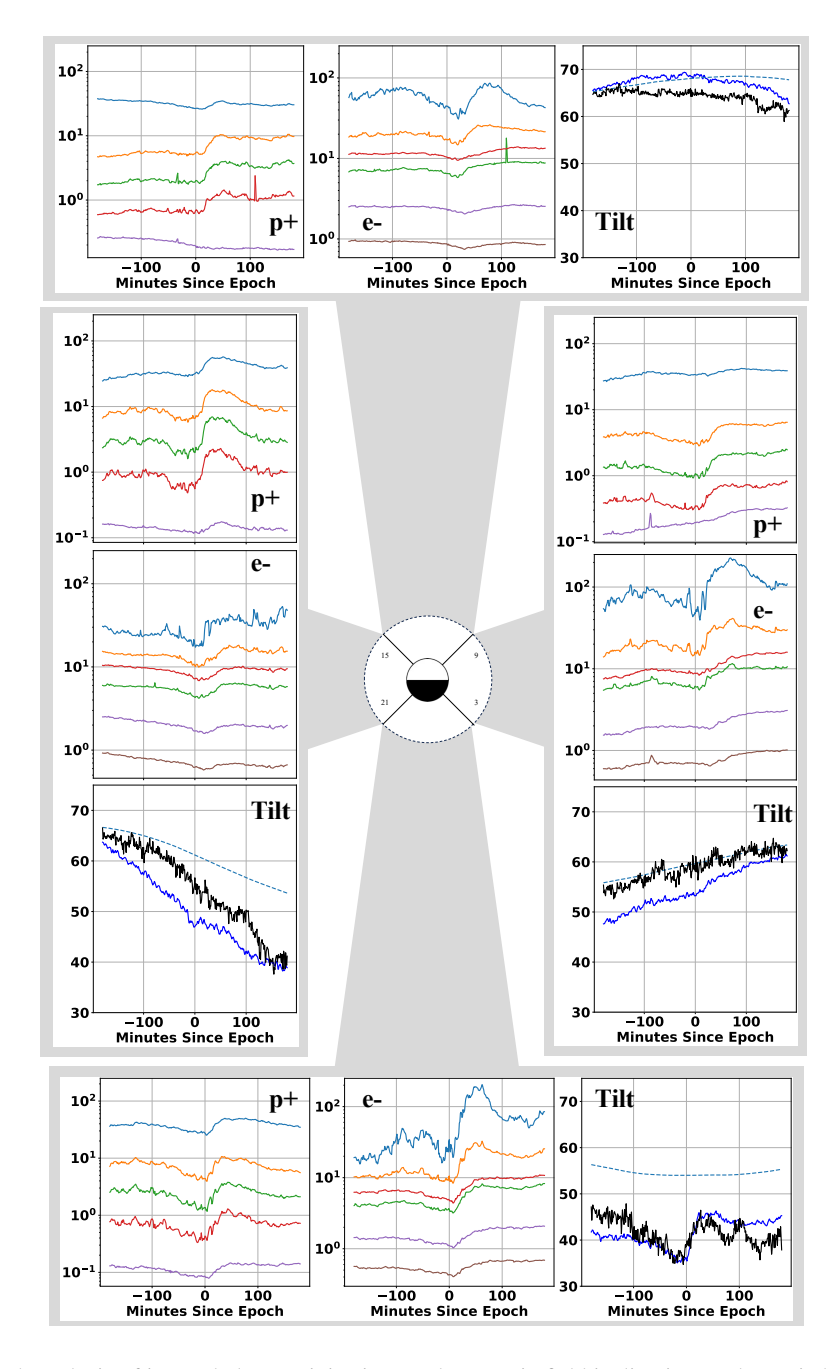


Figure 3. Superposed epoch analysis of ion and electron injections and magnetic field inclination angle carried out separately in four local time quadrants. The proton channels are 92, 138, 206, and 316 keV, and the electron channels are 125, 183, 266, 396, 612, and 908 keV (from top to bottom of each panel, respectively, as the flux values decrease with increasing energy). The field inclination panels show the results from GOES magnetometers and LANL distribution function calculations and Tsyganenko (1989) model for Kp = 2 for reference.



150

155

160



nearly simultaneous and almost similar intensity particle injections at all four MLT sectors, with higher dispersion patterns observed on the dayside. However, quantifying the exact level of dispersion remains difficult, as the satellite configurations vary from event to event, and the dispersion timings have to be done for each individual event rather than examining the superposition which combines a range of conditions and configurations.

The superposed epoch analysis in Figure 3 highlights a key characteristic of sawtooth events: While energetic proton injections occur across all MLT sectors, significant magnetic field dipolarization is only observed in the midnight sector. This suggests that the injections are a global phenomenon, likely driven by large-scale convection and tail reconnection, but the magnetic field tilt does not necessarily exhibit a corresponding global reconfiguration.

The absence of strong dipolarization in the noon, dawn, and dusk sectors indicates that the large-scale magnetic field structure remains relatively stable outside the midnight region. This finding challenges interpretations that sawtooth events involve a system-wide restructuring of the magnetosphere. If large-scale dipolarization were the primary driver of sawtooth oscillations, we would expect synchronous dipolarization signatures at all MLT sectors. Instead, our findings support a scenario in which particle injections originate from nightside reconnection in a substorm-like manner, rather than from a global magnetospheric instability (Henderson, 2016).

The stretched field configuration shows a decrease and subsequent increase in the dawn and dusk plasma sheet before and after onset. This pattern follows the expected diurnal variation, as a six-hour superposed epoch window captures the daily variation around the geostationary orbit. However, the night sector exhibits a clear dipolarization occurring approximately at the injection onset.

On the dayside, the magnetic configuration corresponds to the quiet time one before the injection onset, followed by a subsequent (minor) stretching of the magnetic field. This contradicts the idea that particle injections result from a compression-driven inward transport of plasma from the dayside magnetopause. If magnetopause pressure pulses were responsible for inward particle transport, we would expect the dayside field to become compressed after onset, opposite to the observed effect. This finding further reinforces the idea that the sawtooth injection particles originate from periodic reconnection in the magnetotail transported by strongly enhanced convection.

6 Conclusions

We have created a dataset of sawtooth events for solar cycle 24 that shows similar occurrence frequency characteristics to prior work from solar cycle 23. Our superposed epoch analysis shows that the injections around the globe are near-simultaneous (global), but that the strong field dipolarizations is a repeatable feature only in the midnight sector (not global). The interval between the teeth in the event sequence is similar to values found for substorms both in observations and conceptual models (Borovsky and Yakymenko, 2017; Freeman and Morley, 2004). These results support a picture in which sawtooth events are created by magnetotail reconnection and very fast convection in the near-geostationary region.



185



Author contributions. C.C. DiMarco (CDiM): Conceptualization, Methodology, Software, Analysis, Investigation, Data curation, Visualization, Writing—original draft, Writing and editing. T.I. Pulkkinen (TIP): Conceptualization, Methodology, Supervision, Writing and editing, Funding acquisition. M.G. Henderson (MGH): Data Resources, Supervision. All authors approved the final manuscript.

Competing interests. The authors declare no competing interests.

175 Code and data availability. The sawtooth event catalog used in this study is provided in the Supplement (supplement.pdf). The analysis code and processing scripts used to generate all figures and statistics in this article will be archived on Zenodo and released upon final publication; the DOI will be inserted here at that time. All observational data analyzed in this work are third-party archives and are not generated by the authors: (i) LANL GEOGRID energetic particle data from geostationary orbit, accessible from Los Alamos National Laboratory under data-use agreements; (ii) GOES magnetometer data available from NOAA/NCEI and via NASA CDAWeb; and (iii) the OMNI SYM-H index available from NASA CDAWeb. Formal access routes and credits for these data sets are listed in the Acknowledgements.

Acknowledgements. We acknowledge Los Alamos National Laboratory for access to the GEOGRID energetic particle data used in this study and thank the data providers and instrument teams for sustained operations and curation. We acknowledge NOAA/NCEI and NASA's Space Physics Data Facility (CDAWeb) for access to GOES magnetometer data and the OMNI SYM-H index. CDiM and TIP acknowledge support from NASA grant 80NSSC21K1675. The authors disclose that generative AI was used only for language editing and formatting assistance; all scientific content, analyses, and conclusions were produced and verified by the authors. We thank Joseph Borovsky and Christian Lao for fruitful discussion and guidance during this project.





References

190

195

200

- Baker, D. N., Pulkkinen, T. I., Angelopoulos, V., Baumjohann, W., and McPherron, R. L.: Neutral line model of substorms: Past results and present view, Journal of Geophysical Research: Space Physics, 101, 12 975–13 010, https://doi.org/https://doi.org/10.1029/95ja03753, 1996.
- Bame, S. J., McComas, D. J., Thomsen, M. F., Barraclough, B. L., Elphic, R. C., Glore, J. P., Gosling, J. T., Chavez, J. C., Evans, E. P., and Wymer, F. J.: Magnetospheric plasma analyzer for spacecraft with constrained resources, Review of Scientific Instruments, 64, 1026–1033, https://doi.org/10.1063/1.1144173, 1993.
- Belian, R. D., Gisler, G. R., Cayton, T., and Christensen, R.: High-Zenergetic particles at geosynchronous orbit during the Great Solar Proton Event Series of October 1989, Journal of Geophysical Research, 97, 16897, https://doi.org/10.1029/92ja01139, 1992.
 - Borovsky, J., Birn, J., and Ridley, A.: Unusual Solar Wind Associated with Global Sawtooth Oscillations: CCMC Simulations of the Magnetosphere, in: Living With a Star Workshop, https://lasp.colorado.edu/sdo/meetings/session_1_2_3/presentations/session3/3_09_Borovsky. pdf, 2004.
- Borovsky, J. E. and Yakymenko, K.: Substorm occurrence rates, substorm recurrence times, and solar wind structure, Journal of Geophysical Research: Space Physics, 122, 2973–2998, https://doi.org/10.1002/2016ja023625, 2017.
- Borovsky, J. E., Lavraud, B., and Kuznetsova, M. M.: Polar cap potential saturation, dayside reconnection, and changes to the magnetosphere, Journal of Geophysical Research Atmospheres, 114, https://doi.org/10.1029/2009ja014058, 2009.
- Brambles, O. J., Lotko, W., Zhang, B., Wiltberger, M., Lyon, J., and Strangeway, R. J.: Magnetosphere Sawtooth Oscillations Induced by Ionospheric Outflow, Science, 332, 1183, https://doi.org/10.1126/science.1202869, 2011.
- Cai, X. and Clauer, C. R.: Investigation of the period of sawtooth events, Journal of Geophysical Research: Space Physics, 114, n/a–n/a, https://doi.org/10.1029/2008ja013764, 2009.
 - Cai, X., Zhang, J.-C., Clauer, C. R., and Liemohn, M. W.: Relationship between sawtooth events and magnetic storms, Journal of Geophysical Research: Space Physics, 116, n/a–n/a, https://doi.org/10.1029/2010ja016310, 2011.
- Chen, Y., Cunningham, G., and Henderson, M.: Determination of errors in derived magnetic field directions in geosynchronous orbit: results from a statistical approach, Annales Geophysicae, 34, 831–843, https://doi.org/10.5194/angeo-34-831-2016, 2016.
 - Delzanno, G. L. and Borovsky, J. E.: The Need for a System Science Approach to Global Magnetospheric Models, Frontiers in Astronomy and Space Sciences, 9, https://doi.org/10.3389/fspas.2022.808629, 2022.
 - Freeman, M. P. and Morley, S. K.: A minimal substorm model that explains the observed statistical distribution of times between substorms, Geophysical Research Letters, 31, https://doi.org/10.1029/2004gl019989, 2004.
- Fung, S. F., Tepper, J. A., and Cai, X.: Magnetospheric state of sawtooth events, Journal of Geophysical Research: Space Physics, 121, 7860–7869, https://doi.org/10.1002/2016ja022693, 2016.
 - Henderson, M. G.: Recurrent embedded substorms during the 19 October 1998 GEM storm, Journal of Geophysical Research: Space Physics, 121, 7847–7859, https://doi.org/10.1002/2015JA022014, 2016.
- Henderson, M. G., Reeves, G. D., Skoug, R., Thomsen, M. F., Denton, M. H., Mende, S. B., Immel, T. J., Brandt, P. C., and Singer, H. J.: Magnetospheric and auroral activity during the 18 April 2002 sawtooth event, Journal of Geophysical Research, 111, https://doi.org/10.1029/2005ja011111, 2006.





- Kilpua, E. K. J., O, L. C., G, L. J., and Li, Y.: Interplanetary coronal mass ejections in the near-Earth solar wind during the minimum periods following solar cycles 22 and 23, Annales Geophysicae, 29, 1455–1467, https://doi.org/https://doi.org/10.5194/angeo-29-1455-2011, 2011.
- Lee, D.-Y.: Sawtooth oscillations directly driven by solar wind dynamic pressure enhancements, Journal of Geophysical Research, 109, https://doi.org/10.1029/2003ja010246, 2004.
 - Papitashvili, N., Bilitza, D., and King, J.: OMNI: A Description of Near-Earth Solar Wind Environment, in: 40th COSPAR Scientific Assembly, 2-10 August, 2014, Moscow, Russia, vol. 40, pp. C0.1–12–14, 2014.
- Pulkkinen, T. I., Ganushkina, N. Y., Tanskanen, E. I., Kubyshkina, M., Reeves, G. D., Thomsen, M. F., Russell, C. T., Singer, H. J., Slavin,
 J. A., and Gjerloev, J.: Magnetospheric current systems during stormtime sawtooth events, Journal of Geophysical Research: Space Physics, 111, https://doi.org/10.1029/2006ja011627, 2006.
 - Pulkkinen, T. I., Partamies, N., McPherron, R. L., Henderson, M., Reeves, G. D., Thomsen, M. F., and Singer, H. J.: Comparative statistical analysis of storm time activations and sawtooth events, Journal of Geophysical Research: Space Physics, 112, n/a–n/a, https://doi.org/10.1029/2006ja012024, 2007.
- Pulkkinen, T. I., Palmroth, M., Koskinen, H. E. J., Laitinen, T. V., Goodrich, C. C., Merkin, V. G., and Lyon, J. G.: Magnetospheric modes and solar wind energy coupling efficiency, Journal of Geophysical Research, 115, 2010.
 - Singer, H. J., Matheson, L., Grubb, R., Newman, A., and Bouwer, S. D.: Monitoring Space Weather with the GOES Magnetometers, in: SPIE Conference Proceedings, GOES-8 and Beyond, edited by Washwell, E. R., vol. 2812, pp. 299–308, 1996.
- Thomsen, M. F., McComas, D. J., Reeves, G. D., and Weiss, L. A.: An observational test of the Tsyganenko (T89a) model of the magnetospheric field, Journal of Geophysical Research: Space Physics, 101, 24827–24836, https://doi.org/https://doi.org/10.1029/96ja02318, 1996.
 - Tsyganenko, N.: A magnetospheric magnetic field model with a warped tail current sheet, Planetary and Space Science, 37, 5–20, https://doi.org/10.1016/0032-0633(89)90066-4, 1989.
- Wang, X., Chen, Y., and Tóth, G.: Simulation of Magnetospheric Sawtooth Oscillations: The Role of Kinetic Reconnection in the Magnetotail, Geophysical Research Letters, 49, https://doi.org/10.1029/2022gl099638, 2022.